Probing Photophysical and Photochemical Processes of Benzoic Acid from ab Initio Calculations

Juan Li, Feng Zhang, and Wei-Hai Fang*

Department of Chemistry, Beijing Normal University, Beijing 100875, China

Received: May 29, 2005; In Final Form: July 11, 2005

The CASSCF and DFT methods have been used to determine geometric and electronic structures of the benzoic acid monomer in the S_0, S_1, S_2, T_1, and T_2 electronic states. The $S_1/T_2/T_1$ three-surface intersection was found by the state-averaged CASSCF calculations, which, in combination with features of the five lowest electronic states, provides new insights into photophysical processes of the benzoic acid monomer. The potential energy profiles of the α C−C and C−O bond fissions as well as decarboxylation reaction in different electronic states have been determined for the benzoic acid monomer. The α C−O bond cleavage starts from the T_2 state and leads to the fragments of $C_6H_5CO(\tilde{X}^2A')$ and $OH(\tilde{X}^2\Pi)$ in the ground state, which is predicted to be the most possible channel upon photoexcitation of the benzoic acid monomer at 270 nm or shorter wavelengths.

Introduction

Benzoic acid is the simplest aromatic carboxylic acid and its dimer is established as the benchmark system for studying proton transfer in the hydrogen bonds in the condensed phase. The proton transfer dynamics in the dimer has been extensively investigated with NMR,[1−5] vibrational spectroscopy,[6−10] optical spectroscopy,[11,12] and diffraction techniques.[13,14] Tunneling dynamics of double proton transfer in benzoic acid dimer in the gas and condensed phases have been explored from the theoretical viewpoint.[15] A semiclassical method was developed and applied to determine the ground-state tunneling splittings of carboxylic acid dimers and their fully deuterated analogues.[16]

Benzoic acid dimer serves as a prototypical system for modeling the unusual spectral behavior of the hydride stretch fundamental. High-resolution ultraviolet spectroscopy has been used to investigate the rotationally resolved excitation spectrum of the first singlet−singlet transition in the benzoic acid dimer.[17] The structure of the dimer in the ground state is determined to be linear, while in the excited S_1 state it is slightly bent. Vibrational spectra of several isotopomers of benzoic acid crystals have been recorded by inelastic neutron scattering and are compared with spectra calculated for different potential energy surfaces.[10] Large anharmonic effects associated with the pair of cooperatively strengthened OH···O═C hydrogen bonds produce complicated infrared spectra in which the OH stretch oscillator strength is spread over hundreds of wavenumbers, resulting in a complicated band sub-structure.[18] The IR absorption spectrum of the jet-cooled benzoic acid monomer and dimer have been recorded throughout the 500−1900 cm^{-1} range via ion dip spectroscopy.[19] Laser-induced dispersed fluorescence spectra of the benzoic acid dimer in the cold environment of supersonic jet expansion have been reinvestigated with improved spectral resolution of measurements.[20]

Derivatives of benzoic acid and its complexes with water or other organic acids have been the subject of numerous experimental and theoretical studies. The permanent dipole moment of π-aminobenzoic acid has been measured[21] and calculated at various theoretical levels.[22] Supersonically cooled *p*- and *m*-aminobenzoic acids were studied using one-color resonantly enhanced multiphoton ionization and two-color zero kinetic energy (ZEKE) photoelectron spectroscopy.[23,24] Two conformational isomers of 3-fluorobenzoic acid dimer have been identified in a supersonic jet expansion by use of laser-induced fluorescence excitation (FE), UV−UV hole-burning, and dispersed fluorescence (DF) spectroscopic methods.[25] A 1:1 mixed dimer between acetic acid and benzoic acid has been chosen as the molecular model to investigate the influence of the methyl rotation on vibrational dynamics in the phenyl ring over a long range mediated by the hydrogen-bonded interface.[26] Spectroscopic properties of the *p*-, *o*-, and *m*-aminobenzoic acid complexes with water have been characterized by two-color resonantly enhanced multiphoton ionization spectroscopy.[27,28]

The structure and properties of the benzoic acid monomer is basic, but important, for understanding the complex proton dynamics of the benzoic acid dimer and its complexes with other molecules. However, there is a general lack of information on structure and reactivity of the benzoic acid monomer, especially for the monomer in the excited electronic states. It is surprising that only a few theoretical and experimental studies have been devoted to the benzoic acid monomer, and most of them predate 1991. The monomer of benzoic acid was found to show phosphorescence alone with a high quantum yield.[29] It was inferred that intersystem crossing to the lowest triplet occurs very efficiently in the benzoic acid monomer. Sensitized phosphorescence excitation spectroscopy was used to observe the electronic excited states of the benzoic acid monomer in supersonic jets.[30] The two sharp bands at 35 923 and 35 943 cm^{-1} were assigned to the origins of the two rotational isomers of the benzoic acid monomer. The technique of laser desorption followed by jet cooling has been used to identify the $S_0 \rightarrow S_1$ absorption spectrum of the benzoic acid monomer in the gas phase.[31] The $S_0 \rightarrow S_1$ band origin was determined to locate at 35 960 cm^{-1} and the rate of the intersystem crossing to triplet

* Address correspondence to this author. Phone: +86-10-58805382. Fax: +86-10-5880-2075. E-mail: fangwh@bnu.edu.cn.

10.1021/jp052837s CCC: $30.25
Published on Web 08/06/2005

state was inferred to be 1.2×10^{12} s^{-1}. Frequencies and intensities of the IR active modes for the monomer were determined from ion dip spectroscopy and density functional calculation.[19] In addition, a few experimental and theoretical investigations[32,33] have been performed to probe the decarboxylation mechanisms of benzoic acid and its complexes with water.

In the present work, we report a complete active space self-consistent-field study on structures and reactivity of the benzoic acid monomer in the ground and excited states, which enable a fuller understanding of the complex proton-transfer dynamics in the benzoic acid dimer. An intersection structure of the $^1n\pi^*$, $^3n\pi^*$, and $^3\pi\pi^*$ states was determined, which gives a clear explanation on photophysical processes of the benzoic acid monomer. Three reaction channels,

$$C_6H_5COOH \rightarrow C_6H_6 + CO_2 \quad (1)$$

$$\rightarrow C_6H_5CO + OH \quad (2)$$

$$\rightarrow C_6H_5 + COOH \quad (3)$$

have been explored for benzoic acid in the ground and excited states, which is the extension of our previous studies on photodissociation dynamics of formic and acetic acids.[34−36] A phenyl substitution may change the dissociation mechanism of aliphatic carboxylic acids, due to the conjugation interaction between the phenyl ring and the carboxylic group in aromatic carboxylic acids. We believe that the present study provides new insights into photophysics and photochemistry of aromatic carboxylic acids.

Computational Details

The five lowest electronic states (S_0, T_1, T_2, S_1, S_2) of the benzoic acid monomer have been studied with different ab initio methods. The stationary structures on the S_0 and T_1 surfaces were optimized at the MP2, B3LYP, and CASSCF levels of theory, while only the CASSCF method was used to determine the stationary structures on the potential energy surfaces of the T_2, S_1, and S_2 states. Once convergence has been reached, the harmonic frequencies were examined at this point to confirm the optimized geometry to be a true minimum or first-order saddle point. The selection of the active space is a crucial step for the CASSCF calculation. From the viewpoint of the localized picture of molecular orbitals, the active space should be composed of the three π and three π^* orbitals in the aromatic ring, the C═O π and π^* orbitals, and the oxygen nonbonding orbital in the C═O group. An active space with 10 electrons in 8 orbitals is employed for the present CASSCF calculations, referred to as CAS(10,8) hereafter, with one of the π^* orbitals excluded from the active space. All the calculations were carried out with the Gaussian 03 program package.[37]

On the basis of the calculated relative energies and frequencies for the stationary structures, as well as the energy gradients and spin−orbit coupling matrix element at the intersection structure, the rate constants for the adiabatic and nonadiabatic unimolecular processes are calculated with the RRKM theory of rate. The rate constant of the adiabatic unimolecular reaction can be expressed as[38,39]

$$k(E) = \frac{1}{h}\frac{E}{s}\frac{\sum_n h(E - \epsilon_n^{\ddagger})}{\sum_n h(E - \epsilon_n)}$$

where E is the total energy of an isolated molecule, $\epsilon_n^{\ddagger}$ and ϵ_n are respectively the vibrational energy levels of the transition state and the reactant molecule, and $h(x)$ is the usual step-function

$$h = \begin{cases} 0, x < 0 \\ 1, x > 0 \end{cases}$$

A simple way to include the nonadiabatic effect is to consider it as a factor of transition probability, just like Miller dealing with the tunneling effect.[40] The expression for the nonadiabatic unimolecular rate constant is in form of

$$k(E) = \frac{1}{h}\frac{E}{s}\frac{\sum_n P(E - \epsilon_n^{\ddagger})}{\sum_n h(E - \epsilon_n)}$$

The hopping probability P is calculated with the expression developed by Delos,[41]

$$P_{\text{Delos}}(E - \epsilon_n) = 4\pi^2 V_{12}^2 \left(\frac{2\mu_h}{\hbar^2 F \Delta F}\right)^{2/3} A_i^2\left[(E - \epsilon_n)\left(\frac{2\mu_h \Delta F^2}{\hbar^2 F^4}\right)^{1/3}\right]$$

where V_{12} is the matrix element that couples the two adiabatic surfaces, μ_h is the effective reduced mass, ΔF is the norm of difference of the gradients on the two crossing surfaces, $|\partial V_1/\partial q - \partial V_2/\partial q|$, and F is the geometric mean of the norms of the two gradients, $\sqrt{|\partial V_1/\partial q| \times |\partial V_2/\partial q|}$.

Results and Discussion

Geometric and Electronic Structures. Geometric structures of the C_6H_5COOH molecule in the lowest five electronic states (S_0, S_1, T_1, S_2, and T_2) were optimized at the CAS(10,8)/cc-pVDZ level. Meanwhile, the S_0 and T_1 structures were determined by the MP2 and B3LYP optimizations with the cc-pVDZ basis set. The optimized structures are shown in Figure 1 where the atom labeling scheme and the key bond parameters are given. Detailed structural parameters are available in the Supporting Information. Two minimum-energy structures, referred to as $C_6H_5COOH(S_0)$-a and $C_6H_5COOH(S_0)$-b hereafter, were found for benzoic acid in the ground state. All the atoms in $C_6H_5COOH(S_0)$-a are coplanar, while $C_6H_5COOH(S_0)$-b has a nonplanar geometry with the H15−O14−C12−C1 dihedral angle of 11.5° at the MP2/cc-pVDZ level. The C−C bond lengths in the aromatic ring are predicted to be almost equal with a value of about 1.40 Å for $C_6H_5COOH(S_0)$-a and $C_6H_5COOH(S_0)$-b, which shows that the conjugation interaction in the aromatic ring is well described by the MP2, B3LYP, and CAS(10,8) calculations. There exists a strong p−π conjugation interaction in the carboxylic group of $C_6H_5COOH(S_0)$-a, but the interaction between the aromatic ring and the carboxylic group is weaker in the $C_6H_5COOH(S_0)$-a and $C_6H_5COOH(S_0)$-b structures. $C_6H_5COOH(S_0)$-a is more stable with the relative energy of 6.6 kcal/mol for $C_6H_5COOH(S_0)$-b. A transition state of $TSab(S_0)$ was found on the isomerization pathway from $C_6H_5COOH(S_0)$-a to $C_6H_5COOH(S_0)$-b and the barrier height is 11.6 kcal/mol at the MP2/cc-pVDZ level of theory. The intramolecular hydrogen bond in the $C_6H_5COOH(S_0)$-a structure is mainly responsible for the relatively high barrier on the OH rotational isomerization pathway from $C_6H_5COOH(S_0)$-a to $C_6H_5COOH(S_0)$-b.

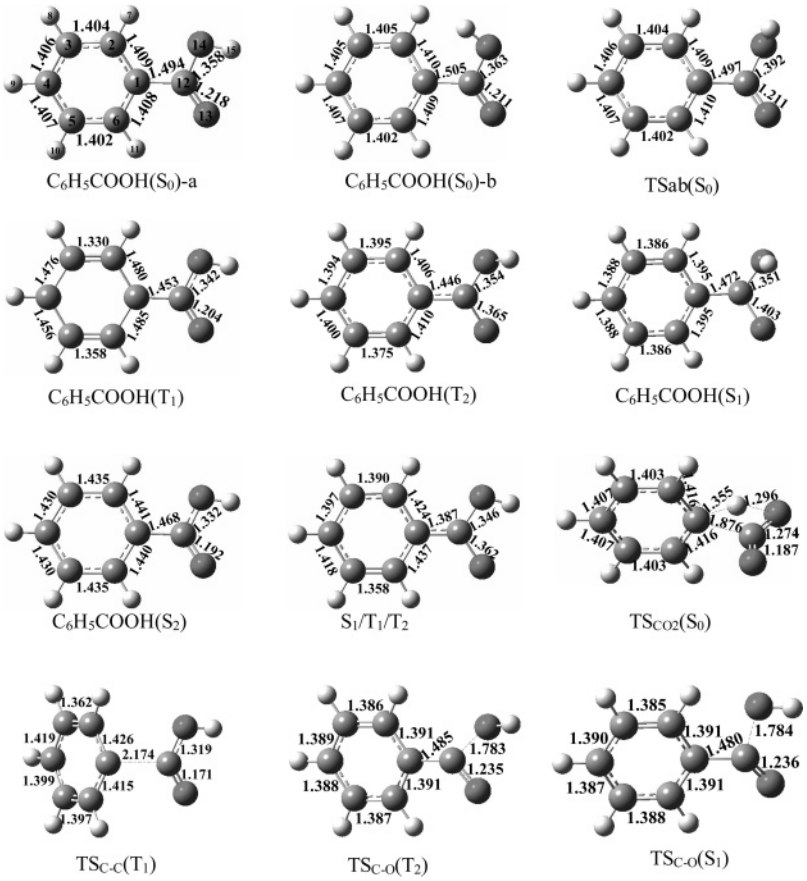

Figure 1. Schematic structures of the stationary and intersection points on different electronic states, along with the selected MP2 bond parameters for the S_0 structures and the CAS(10,8) bond parameters for the excited-state structures (bond lengths in Å). The atom labeling is given in the $C_6H_5COOH(S_0)$-a structure.

One minimum-energy structure, $C_6H_5COOH(T_1)$, was found on the lowest triplet surface of benzoic acid by the B3LYP and CAS(10,8) calculations. $C_6H_5COOH(T_1)$ has a planar geometry, which is similar to the $C_6H_5COOH(S_0)$-a structure. The structure of the carboxylic group is nearly unchanged from $C_6H_5COOH(S_0)$-a to $C_6H_5COOH(T_1)$. The C3−C2 and C6−C5 bond lengths in $C_6H_5COOH(T_1)$ are 1.330 and 1.358 Å, respectively, indicating C═C double bond character, while the other C−C bonds in the aromatic ring are mainly of single bond character. Actually, the T_1 state of C_6H_5COOH is a diradical with the two singly occupied electrons distributed on the C1 and C4 atoms. The CAS(10,8) wave functions and their electron populations clearly show that the T_1 state of C_6H_5COOH originates from the $\pi \rightarrow \pi^*$ excitation in the aromatic ring. This confirms the experimental speculation[31] that the lowest triplet state is a $^3\pi\pi^*$ state for the benzoic acid monomer. With respect to the S_0 zero level, the T_1 state has a relative energy of 73.8 and 75.5 kcal/mol at the CAS(10,8)/cc-pVDZ and B3LYP cc-pVDZ levels, respectively.

The CAS(10,8) optimized structure of the first excited singlet state, $C_6H_5COOH(S_1)$, is plotted in Figure 1, from which one can see that the S_1 state is quite different from the T_1 state in structure. The C−C bond lengths in the aromatic ring are less influenced by an electronic excitation from S_0 to S_1. The largest change is associated with the C12−O13 bond, which is a double bond in S_0 and T_1 and becomes a single bond in the S_1 structure. The CASSCF wave functions and their electron populations clearly show that the S_1 state arises from an electronic excitation located in the C═O group and is of $^1n\pi^*$ character. The adiabatic excitation energy from S_0 to S_1 was predicted to be 32 002.6 cm^{-1} (91.5 kcal/mol) at the CAS(10,8)/cc-pVDZ level and the energy difference between S_1 and T_1 is 17.7 kcal/mol. Unlike the T_1 state, the T_2 structure is similar to that of the S_1 state. The structural similarity between T_2 and S_1 predicts that the T_2 state is of $^3n\pi^*$ character, which is confirmed by the CASSCF wave functions and their electron populations for the T_2 state. With respect to the S_0 zero level, the $T_2(^3n\pi^*)$ state has a relative energy of 90.0 kcal/mol at the CAS(10,8)/cc-pVDZ level, which is 16.2 kcal/mol higher than the $T_1(^3\pi\pi^*)$ state, but 1.5 kcal/mol lower than the $S_1(^1n\pi^*)$ state in energy. The T_2 state of the benzoic acid monomer was experimentally inferred to be $^3n\pi^*$ in nature, which lies between the S_1 and T_1 states in energy.[30,31]

A planar S_2 structure, $C_6H_5COOH(S_2)$, was optimized and confirmed to be minimum by the CAS(10,8) calculations. In comparison with the S_0 structure, the carboxylic group is nearly unchanged in $C_6H_5COOH(S_2)$, but the C−C bond lengths in the aromatic ring are increased to ∼1.44 Å in $C_6H_5COOH(S_2)$ from ∼1.40 Å in the S_0 structure. The structural features of $C_6H_5COOH(S_2)$ reveal that the S_2 state is $^1\pi\pi^*$ in nature. The further evidence for this comes from the CASSCF wave functions and their electron populations for the S_2 state. The $\pi \rightarrow \pi^*$ excitation is mainly localized in the aromatic ring, and the lengthening of the C−C bonds in the ring exhibits characteristics of a $\pi \rightarrow \pi^*$ transition, where the aromatic ring attempts to reduce its π-bonding character upon excitation. The adiabatic excitation energy from S_0 to S_2 is calculated to be 35 220.3 cm^{-1} (100.7 kcal/mol) at the CAS(10,8)/cc-pVDZ level, which is comparable to the bond origin of 35 923−35 960 cm^{-1} (∼102.7 kcal/mol) observed experimentally for the benzoic acid monomer.[30,31] The $S_2(^1\pi\pi^*)$ state is 10.8 kcal/mol higher than the $S_1(^1n\pi^*)$ state in energy.

All the experimental efforts to find the $^1n\pi^*$ state in the energy region below the $^1\pi\pi^*$ state were in vain for the benzoic acid monomer.[30,31] The lack of experimental evidence led to the assumption that there is no $^1n\pi^*$ state below the $^1\pi\pi^*$ state and the latter is the lowest singlet excited state. This assumption is not supported by the present calculations, which show that the $^1n\pi^*$ minimum is lower in energy than the $^1\pi\pi^*$ minimum. The S_1 state was assigned to $^1\pi\pi^*$ in nature for the monomer in the previous studies,[30,31,42,43] which is based on the absorption or fluorescence excitation spectroscopy in the Franck−Condon (FC) region. The vertical excitation energies from the ground state to the three lowest excited singlet states were calculated to be respectively 39 522.3, 40 886.3, and 45 573.0 cm^{-1} with the time-dependent DFT method, in conjugation with the cc-pVDZ basis set. Again, the lowest excited singlet state in the FC region is predicted to be the $^1n\pi^*$ state with an oscillator strength of 0.0002. The other two excited singlet states are of $^1\pi\pi^*$ nature with oscillator strengths of 0.015 and 0.18. The oscillator strength of the $S_0 \rightarrow {}^1\pi\pi^*$ transition is 75−900 times larger than that for the $S_0 \rightarrow {}^1n\pi^*$ absorption, which is probably the reason the $^1n\pi^*$ state was not observed experimentally in the energy region below the $^1\pi\pi^*$ state.

The benzoic acid monomer is nonfluorescent but phosphorescent. However, the dimer is fluorescent and phosphorescent. The emission properties of the monomer and dimer were explained with a simple energy level diagram in the previous studies.[30,31] The basic idea is that the first excited singlet state is $^1\pi\pi^*$ in nature, which is nearly degenerate with the $^3n\pi^*$ state. This makes the $^1\pi\pi^* \rightarrow {}^3\pi\pi^*$ intersystem crossing via the $^3n\pi^*$ state very efficient in the monomer.[31] In the dimer, on the other hand, the $^3n\pi^*$ state is pushed up in energy whereas the $^1\pi\pi^*$ state is pushed down in energy relative to the situation in the monomer. As a result, the $^1\pi\pi^* \rightarrow {}^3\pi\pi^*$ intersystem crossing rate is largely reduced for the dimer. The above explanations are based on the assignment of the S_1 state as $^1\pi\pi^*$ in nature for the monomer. However, the S_1 state is confirmed to be $^1n\pi^*$ in nature by the present calculations. Thus, it is necessary to carry out further study to elucidate the emission properties of the benzoic acid monomer and dimer.

The $S_1/T_1/T_2$ Three-Surface Intersection. To explore photophysical processes of the benzoic acid monomer, we searched for the surface crossing points between the singlet and triplet states as well as the crossing points of two triplet states. The T_1 and T_2 surface intersection (T_1/T_2) in the Franck−Condon (FC) region was optimized with the state-averaged CAS(10,8) approach, while the S_1 and T_1 crossing (S_1/T_1) structure was determined by using Slater determinants in the state-averaged CAS(10,8) calculations. It was found that T_1/T_2 and S_1/T_1 crossing points are indistinguishable in structure and the two crossing points are almost equal in energy. Actually, the S_1, T_1, and T_2 surfaces intersect at the same region, referred to as $S_1/T_1/T_2$. The optimized $S_1/T_1/T_2$ structure is shown in Figure 1 along with the selected CAS(10,8) bond parameters. The detailed structures and energies for the intersections are available in the Supporting Information. A comparison reveals that the $S_1/T_1/T_2$ geometric structure lies between the $T_1(^3\pi\pi^*)$ and $S_1(^1n\pi^*)$ geometric structures. The CAS(10,8) wave functions and their electron populations show that the $S_1/T_1/T_2$ structure is a diradical in nature and the two unpaired electrons are mainly distributed on the C1 and O13 atoms, respectively. As pointed out before, the T_1 state of C_6H_5COOH is a diradical with the two singly occupied electrons distributed on the C1 and C4 atoms, respectively. The S_1 and T_2 states are also of diradical nature, but the two unpaired electrons are located on the C12 and O13 atoms, respectively. The localized pictures of the $S_1(T_2)$, $S_1/T_1/T_2$, and T_1 electronic structures are summarized in Scheme 1. It is obvious that the $S_1/T_1/T_2$ three-surface intersection is a bridge that connects the $S_1(^1n\pi^*)$ state on one side and the $T_1(^3\pi\pi^*)$ state on the other side.

SCHEME 1

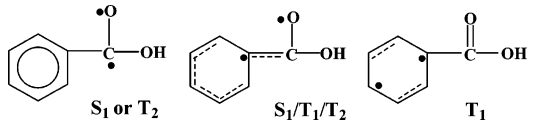

SCHEME 2

$$S_2(^1\pi\pi^*) \xrightarrow{IC} S_1(^1n\pi^*) \xrightarrow[S_1/T_1/T_2]{ISC} T_1(^3\pi\pi^*)$$

The $\pi \rightarrow \pi^*$ transition for benzoic acid is mainly localized in the aromatic ring with a deep potential well, and the S_2 direct dissociation proceeds with little probability upon interaction with ultraviolet light. As discussed before, the $S_2(^1\pi\pi^*)$ state is 10.8 kcal/mol higher than the nonplanar $S_1(^1n\pi^*)$ state in energy. The relatively small electronic energy gap between the $S_2(^1\pi\pi^*)$ and the $S_1(^1n\pi^*)$ states leads to a favorable Franck−Condon factor for the $S_2 \rightarrow S_1$ internal conversion. Vibrational analysis shows that there are a number of promoting and accepting modes that couple the $S_2(^1\pi\pi^*)$ and the $S_1(^1n\pi^*)$ states, indicating that the internal conversion from $S_2(^1\pi\pi^*)$ to $S_1(^1n\pi^*)$ takes place with high efficiency. There exists a small difference in the S_1 and $S_1/T_2/T_1$ structures, which results from the redistribution of the conjugation π electrons in the aromatic ring and the carbonyl group. This will not give rise to a substantial change in the energy. The CAS(10,8)/cc-pVDZ calculations predict that the $S_1/T_2/T_1$ structure is 4.7 kcal/mol in energy above the S_1 minimum. In view of the similar structures and small energy difference, the relaxation from the S_1 geometry to the $S_1/T_2/T_1$ region is expected to occur in a vibrational period. The spin−orbit interaction at the $S_1/T_2/T_1$ structure was calculated by using a one-electron approximation for the spin−orbital coupling operator with the effective nuclear charges of Koseki et al.[44] The spin−orbit coupling matrix element was predicted to be 65.1 cm^{-1}, which is used as the V_{12} for calculation of the hopping probability. The nonadiabatic RRKM rate calculation gives a value of 2.7×10^{10} s^{-1} for the $S_1 \rightarrow T_1$ ISC rate constant at the intersection structure. From the observed width of the peaks in the $S_0 \rightarrow S_1$ gas-phase absorption spectrum, an intersystem crossing rate of 1.2×10^{12} s^{-1} was deduced experimentally for the benzoic acid monomer.[31] After photoexcitation to the $S_2(^1\pi\pi^*)$ state, the rapid radiationless processes to the $T_1(^3\pi\pi^*)$ state are summarized in Scheme 2 for C_6H_5COOH, which gives a reasonable explanation why the benzoic acid monomer is nonfluorescent but phosphorescent.

Decarboxylation. Examination of the $C_6H_5COOH(S_0)$ structures in Figure 1 reveals that isomerization from $C_6H_5COOH(S_0)$-a to $C_6H_5COOH(S_0)$-b takes place prior to decarboxylation. The decarboxylation reaction involves a 1,3-H shift of the H15 atom accompanied by a cleavage of the C−C bond. Although a planar geometry was used as the initial guess, the optimized structure of the transition state [$TS_{CO2}(S_0)$] is nonplanar. As shown in Figure 1, the carboxyl group adopts a nearly perpendicular conformation to the aromatic ring in $TS_{CO_2}(S_0)$ structure with the O14−C12−C1−C6 dihedral angle of 103.6°. The barrier to decarboxylation in the ground state was calculated to be 60.6 kcal/mol at the MP2/cc-pVDZ level of theory, including the vibrational zero-point energy correction at the same level, which is close to that from the B3LYP

calculations[32] (58.8−62.0 kcal/mol). However, the barrier (103−116 kcal/mol) was overestimated by the Hartree−Fock calculations with the 3-21G basis set.[33] Due to a high barrier on the pathway, there is little possibility that the decarboxylation of benzoic acid occurs in the ground state at room temperature. The decarboxylation reaction of C_6H_5COOH involves cleavages of the C−C and O−H bonds, formation of the H−C bond, and a large deformation of the O−C−O moiety, simultaneously. It is reasonable to expect that on the excited electronic states the decarboxylation reactions should not be in competition with the photophysical processes discussed above. It can be concluded that decarboxylation reaction does not play an important role in the mechanistic photochemistry of the benzoic acid monomer.

The α C−O Bond Cleavage. C_6H_5COOH may dissociate into C_6H_5CO + OH along the S_0 pathway, which corresponds to cleavage of the C−O bond α to the C═O group. We have made efforts to optimize a transition state for the C−O bond cleavage in the ground state, but optimizations always lead to the dissociation limit of C_6H_5CO + OH. It is evident that no potential barrier above endothermicity exists on the S_0 pathway. The energy of the separated fragments was determined from a supermolecule optimization with the CAS(10,8)/cc-pVDZ approach, which is the same as that for the bound fragments. In this way, the C−O bond cleavage is predicted to be endothermic by 98.7 kcal/mol. On the basis of thermochemical data, the C−O bond cleavage was estimated to be endothermic by 96.8 kcal/mol for HCOOH.[45]

A nonplanar transition state on a triplet pathway, referred to as $TS_{C-O}(T_2)$ in Figure 1, was determined by the CAS(10,8)/cc-pVDZ optimizations. The IRC calculations were done with the $TS_{C-O}(T_2)$ structure as the starting point, which confirms that $TS_{C-O}(T_2)$ connect $C_6H_5COOH(T_2)$ on the reactant side and the fragments of $C_6H_5CO(\tilde{X}^2A')$ and $OH(\tilde{X}^2\Pi)$ on the product side. The barrier height for the α C−O bond fission starting from the T_2 state is 12.2 kcal/mol at the CAS(10,8)/cc-pVDZ level of theory with the zero-point energy correction included at the same level. As shown in Figure 1, a nonplanar transition state, $TS_{C-O}(S_1)$, was found on the excited singlet surface. $TS_{C-O}(S_1)$ and $TS_{C-O}(T_2)$ are very similar in structure. This predicts that $TS_{C-O}(S_1)$ is the transition state governing the $C_6H_5COOH(S_1)$ dissociation into $C_6H_5CO(\tilde{X}^2A')$ and $OH(\tilde{X}^2\Pi)$, which is confirmed by the IRC calculations at the CAS(10,8)/cc-pVDZ level. The α C−O bond cleavage starting from the S_1 state has a barrier of 15.7 kcal/mol at the CAS(10,8)/cc-pVDZ level, which is 3.5 kcal/mol higher than that on the T_2 pathway. The barrier height of the C−O single bond cleavage was not measured for C_6H_5COOH in the low-lying electronic states. The C−O single bond cleavage of CH_3COOH was experimentally estimated to have a barrier of 13−14 kcal/mol on the S_1 pathway,[46−48] which gives us reason to expect that the C−O single bond cleavage for C_6H_5COOH is well described by the present calculations. The potential energy surfaces for the C−O bond cleavages on different electronic states are plotted in Figure 2.

The α C−C Bond Fission. Like the α C−O bond cleavage, no potential barrier above endothermicity exists on the S_0 pathway of the α C−C bond fission. The α C−C bond dissociation energy was predicted to be 109.0 kcal/mol from a supermolecular calculation at the CAS(10,8)/cc-pVDZ level. On the basis of thermochemical data,[49] the α C−C bond cleavage was estimated to be endothermic by 105.2 kcal/mol for C_6H_5COOH. The C−C bond dissociation energy of CH_3COOH was estimated to be 90.2 and 96.3 kcal/mol from heats of formation at 0 K and the CAS(8,7)/cc-pVDZ calculations,[50]

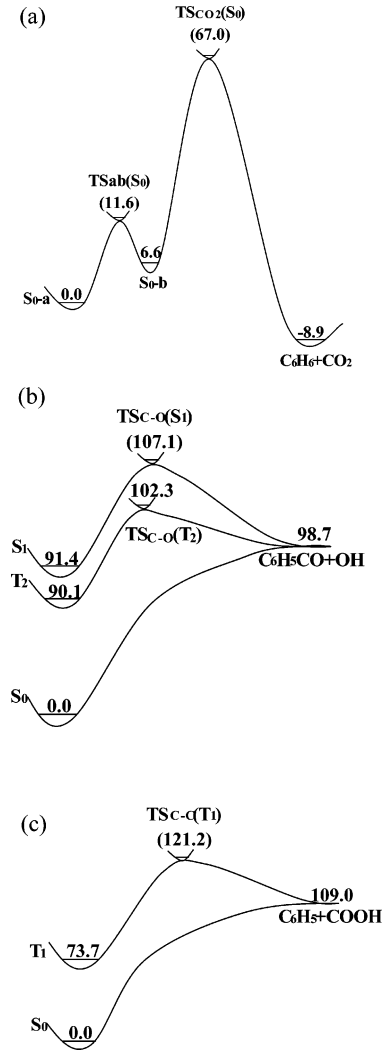

Figure 2. Schematic potential energy surfaces of the decarboxylation process (a), the α C−O fissions (b), and the α C−C bond cleavages (c), along with the relative energies in parentheses (kcal/mol).

respectively. Because of the conjugation interaction between the aromatic ring and the carboxylic group, the α C−C bond in C_6H_5COOH is stronger than the C−C bond in CH_3COOH. This is the reason the α C−C bond fission in the ground state has higher endothermicity in C_6H_5COOH than in CH_3COOH.

A transition state was optimized at the B3LYP and CAS(10,8) levels of theory with the cc-pVDZ basis set, which is confirmed to be the first-order saddle point on the triplet surface. The IRC calculations at the B3LYP and CAS(10,8) levels show that the optimized transition state connects $C_6H_5COOH(T_1)$ in the reactant side and the fragments of $C_6H_5(\tilde{X}^2A')$ and $COOH(\tilde{X}^2A')$ on the product side. This transition state is labeled by $TS_{C-C}(T_1)$ in Figure 1. With respect to the zero-point level of the T_1 state, the α C−C bond fission on the T_1 pathway has a barrier of 35.4 kcal/mol at the B3LYP/cc-pVDZ level and 47.4 kcal/mol at the CAS(10,8)/cc-pVDZ level. The α C−C bond fission along the S_1 pathway leads to the fragments of $C_6H_5(\tilde{X}^2A')$ and $COOH(\tilde{A}^2A)$ in the excited state, which is about 70.7 kcal/mol higher than the fragments of $C_6H_5(\tilde{X}^2A')$ and $COOH(\tilde{X}^2A')$ in the ground state.[51,52] Therefore, the α C−C bond fission along the S_1 pathway is inaccessible in energy upon photoexcitation of C_6H_5COOH in the UV region.

Mechanistic Photodissociation. Irradiation of benzoic acid at ∼270 nm leads to the molecules in the $S_2(^1\pi\pi^*)$ state. The main pathway for the $C_6H_5COOH(^1\pi\pi^*)$ deactivation is internal

conversion to the $S_1(^1n\pi^*)$ state. From this state, there are two possible routes, the direct C−O single bond cleavage through the $TS_{C-O}(S_1)$ transition state and intersystem crossing via the $S_1/T_1/T_2$ intersection. With respect to the S_0 zero level, the $TS_{C-O}(S_1)$ transition state has its relative energy of 107.1 kcal/mol, which is inaccessible in energy upon photoexcitation at wavelengths longer than 267 nm. The $S_1/T_1/T_2$ intersection is 98.1 kcal/mol above the S_0 minimum and the ISC rate at the intersection structure is predicted to be 2.7×10^{10} s^{-1}. It is evident that the direct C−O bond dissociation is not in competition with the ISC processes for the benzoic acid monomer in the S_1 state.

Relative to the S_0 zero level, the α C−C bond cleavage has a barrier of 121.2 kcal/mol on the T_1 pathway, which is inaccessible in energy even at photoexcitation at 248 nm. After relaxation to the T_1 state, the benzoic acid monomer emits phosphorescence only. The α C−C bond cleavage does not play a role in the photochemistry of the benzoic acid monomer. The $S_1 \rightarrow T_2$ ISC can take place with high efficiency, because of the existence of the $S_1/T_1/T_2$ intersection. The C_6H_5COOH molecules that decay to the T_2 state are left with sufficient internal energies to overcome the barrier (12.2 kcal/mol) to the α C−O bond cleavage along the T_2 pathway. On the basis of the CAS(10,8)/cc-pVDZ frequencies and energies for the T_2 minimum and $TS_{C-O}(T_2)$ structures, the adiabatic RRKM theory of rate[38,39] is employed to calculate the rate constant of the C−O single bond cleavage along the T_2 pathway. Only vibrational degrees of freedom are considered in the present calculations with a harmonic approximation. The RRKM rate constant is computed to be 5.2×10^{11} s^{-1} for the C−O bond cleavage with a total angular momentum of $J = 0$ and a total energy of $E = 16.0$ kcal/mol, which corresponds to an energy difference between 270-nm photon and the T_2 vibrational zero level. It can be concluded that the most possible reaction channel is the fission of the α C−O bond from the T_2 state upon photodissociation of the benzoic acid monomer at 270 nm or shorter wavelengths.

Summary

The CASSCF and DFT methods have been used to optimize equilibrium structures of the benzoic acid monomer in the S_0, S_1, S_2, T_1, and T_2 electronic states. On the basis of the calculated adiabatic excitation energies, the CASSCF wave functions, and their electronic populations, the S_1, S_2, T_1, and T_2 states were respectively characterized as $^1n\pi^*$, $^1\pi\pi^*$, $^3\pi\pi^*$, and $^3n\pi^*$ in nature. The $S_1/T_2/T_1$ three-surface intersection structure was found by the state-averaged CASSCF calculations, which, in combination with properties of the S_1, S_2, T_1, and T_2 electronic states, gives a reasonable explanation why the benzoic acid monomer is nonfluorescent but phosphorescent. Since the $S_2 \rightarrow S_1$ internal conversion and the $S_1 \rightarrow T_1$ intersystem crossing take place with high efficiency, there is little probability that the excited-state C_6H_5COOH molecules relax to the ground state via internal conversion or intersystem crossing. The decarboxylation reaction that only can occur on the ground state does not play an important role in the photochemical processes of the benzoic acid monomer. The potential energy profiles of the α C−C and C−O bond fissions in different states have been determined for the benzoic acid monomer. The α C−C bond dissociations along the excited-state pathways are inaccessible in energy upon photoexcitation at 270 nm or longer wavelengths. The α C−O bond fission along the S_1 pathway is not in competition with the ISC processes from S_1 to T_1 or T_2. The C−O bond cleavage starts from the T_2 state and leads to the fragments of $C_6H_5CO(\tilde{X}^2A')$ and $OH(\tilde{X}^2\Pi)$ in the ground state, which is the most possible channel upon photoexcitation of the benzoic acid monomer at 270 nm or shorter wavelengths.

Acknowledgment. This work was supported by grants from the National Natural Science Foundation of China (Grant Nos. 20472011 and 20233020) and from the Major State Basic Research Development Programs (Grant Nos. 2004CB719903 and 2002CB613406).

Supporting Information Available: Structures and energies for all stationary points reported in the present work. This material is available free of charge via the Internet at http://pubs.acs.org.

References and Notes

(1) Meyer, R.; Ernst, R. R. *J. Chem. Phys.* **1990**, *93*, 5518.
(2) Stockli, A.; Meier, B. H.; Meyer, R.; Ernst, R. R. *J. Chem. Phys*. **1990**, *93*, 1502.
(3) Scheurer, C.; Saalfrank, P. *Chem. Phys. Lett*. **1995**, *245*, 201.
(4) Brougham, D. F.; Horsewill, A. J.; Jenkinson, R. I. *Chem. Phys. Lett*. **1997**, *272*, 69.
(5) Xue, Q.; Horsewill, A. J.; Johnson, M. R.; Trommsdorff, H. P. *J. Chem. Phys*. **2004**, *120*, 11107 and references therein.
(6) Nakamura, R.; Machida, K.; Oobatake, M.; Hayashi, S. *Mol. Phys.* **1988**, *64*, 215.
(7) Zelsmann, H. R.; Mielke, Z. *Chem. Phys. Lett.* **1991**, *186*, 501.
(8) Hayashi, S.; Oobatake, M.; Nakamura, R.; Machida, K. *J. Chem. Phys.* **1991**, *94*, 4446.
(9) Fillaux, F.; Limage, M. H.; Romain, F. *Chem. Phys*. **2002**, *276*, 181.
(10) Plazanet, M.; Fukushima, N.; Johnson, M. R.; Trommsdorff, H. P. *J. Chem. Phys*. **2001**, *115*, 3241.
(11) Oppenlander, A.; Rambaud, C.; Trommsdorff, H. P.; Vial, J. C. *Phys. Rev. Lett.* **1989** *63*, 1432.
(12) Rambaud, C.; Oppenlander, A.; Pierre, M. M.; Trommsdorff, H. P.; Vial, J. C. *Chem. Phys*. **1989**, *136*, 335.
(13) Wilson, C. C.; Shankland, N.; Florence, A. J. *Chem. Phys. Lett.* **1996**, *253*, 103.
(14) Wilson, C. C.; Shankland, N.; Florence, A. J. *J. Chem. Soc., Faraday Trans.* **1996**, *92*, 5051
(15) Smedarchina, Z.; Fernandez-Ramos, A.; Siebrand, W. C. *J. Chem. Phys*. **2005**, *122* and references therein.
(16) Tautermann, C. S.; Voegele, A. F.; Liedl, K. R. *J. Chem. Phys*. **2004**, *120*, 631.
(17) Remmers, K.; Meerts W. L.; Ozier, I. *J. Chem. Phys*. **2000**, *112*, 10890.
(18) Florio, G. M.; Zwier, T. S.; Myshakin, E. M. *J. Chem. Phys*. **2003**, *118*, 1735.
(19) Bakker, J. M.; MacAleese, L.; von Helden, G.; Meijer, G. *J. Chem. Phys*. **2003**, *119*, 11180 and references therein.
(20) Nandi, C. K.; Chakraborty, T. *J. Chem. Phys*. **2004**, *120*, 8521 and references therein.
(21) Compagnon, I.; Antoine, R.; Rayane, D. *J. Phys. Chem. A* **2003**, *107*, 3036.
(22) Rubio-Pons, O.; Luo, Y. *J. Chem. Phys*. **2004**, *121*, 157.
(23) He, Y. G.; Wu, C. Y.; Kong, W. *J. Chem. Phys*. **2004**, *121*, 3533.
(24) He, Y. G.; Wu, C. Y.; Kong, W. *J. Chem. Phys*. **2004**, *121*, 8321.
(25) Nandi, C. K.; Hazra, M. K.; Chakraborty, T. *J. Chem. Phys*. **2004**, *121*, 5261.
(26) Nandi, C. K.; Hazra, M. K.; Chakraborty, T. *J. Chem. Phys*. **2004**, *121*, 7562.
(27) He, Y. G.; Wu, C. Y.; Kong, W. *J. Phys. Chem. A* **2005**, *109*, 748.
(28) He, Y. G.; Wu, C. Y.; Kong, W. *J. Phys. Chem. A* **2005**, *109*, 2809.
(29) Baba, H.; Kitamura, M. *J. Mol. Spectrosc*. **1972**, *41*, 302.
(30) Kamei, S.-i.; Abe, H.; Mikami, N.; Ito, M. *J. Phys. Chem.* **1985**, *89*, 3636.
(31) Meijer, G.; de Vries, M. S.; Hunziker, H. E.; Wendt, H. E. *J. Phys. Chem.* **1990**, *94*. 4394.
(32) Li, J.; Brill, T. B. *J. Phys. Chem. A* **2003**, *107*, 2667.
(33) Ruelle, P. *J. Mol. Struct.* (*THEOCHEM*) **1987**, *8*, 158.
(34) Su, H. M.; Kong, F. N.; Fang, W. H.; Liu, R. Z. *J. Chem. Phys.* **2000**, *113*, 1891.
(35) He, H. Y.; Fang, W. H. *J. Am. Chem. Soc.* **2003**, *125*, 16139.
(36) Fang, W. H.; Liu, R. Z.; Zheng, X. M.; Philips, D. L. *J. Org. Chem.* **2002**, *67*, 8407.

(37) Frisch, M. J.; Trucks, G. W.; Schlegel, H. B.; Scuseria, G. E.; Robb, M. A.; Cheeseman, J. R.; Montgomery, J. A.; Jr., T. V.; Kudin, K. N.; Burant, J. C.; Millam, J. M.; Iyengar, S. S.; Tomasi, J.; Barone, V.; Mennucci, B.; Cossi, M.; Scalmani, G.; Rega, N.; Petersson, G. A.; Nakatsuji, H.; Hada, M.; Ehara, M.; Toyota, K.; Fukuda, R.; Hasegawa, J.; Ishida, M.; Nakajima, T.; Honda, Y.; Kitao, O.; Nakai, H.; Klene, M.; Li, X.; Knox, J. E.; Hratchian, H. P.; Cross, J. B.; Adamo, C.; Jaramillo, J.; Gomperts, R.; Stratmann, R. E.; Yazyev, O.; Austin, A. J.; Cammi, R.; Pomelli, C.; Ochterski, J. W.; Ayala, P. Y.; Morokuma, K.; Voth, G. A.; Salvador, P.; Dannenberg, J. J.; Zakrzewski, G.; Dapprich, S.; Daniels, A. D.; Strain, M. C.; Farkas, O.; Malick, D. K.; Rabuck, A. D.; Raghavachari, K.; Foresman, J. B.; Ortiz, J. V.; Cui, Q.; Baboul, A. G.; Clifford, S.; Cioslowski, J.; Stefanov, B. B.; Liu, G.; Liashenko, A.; Piskorz, P.; Komaromi, I.; Martin, R. L.; Fox, D. J.; Keith, T.; Al-Laham, M. A.; Peng, C. Y.; Nanayakkara, A.; Challacombe, M.; Gill, P. M. W.; Johnson, B.; Chen, W.; Wong, M. W.; Gonzalez, C.; Pople, J. A. *Gaussian 03*, Revision C.01; Gaussian, Inc.: Pittsburgh, PA, 2003.

(38) Robbinson, P. J.; Holbrook, K. A. *Unimolecular Reactions*; Wiley: New York, 1972.

(39) Forst, W. *Theory of Unimolecular Reactions*; Academic Press: New York, 1973.

(40) Miller, W. H. *J. Am. Chem. Soc.* **1979**, *101*, 220.

(41) Delos, J. B.; Thorson, W. R. *Phys. Rev. A* **1972**, *6*, 728.

(42) Baum, J. C.; McClure, D. S. *J. Am. Chem. Soc.* **1979**, *101*, 2335.

(43) Baum, J. C. *J. Am. Chem. Soc.* **1980**, *102*, 716.

(44) Koseki, S.; Schmidt, M. W.; Gordon, M. S. *J. Phys. Chem.* **1992**, *96*, 10768.

(45) Su, H.; He, Y.; Kong, F.; Fang, W.-H.; Liu, R.-Z. *J. Chem. Phys.* **2000**, *113*, 1891.

(46) Hunnicutt, S. S.; Waits, L. D.; Guest, J. A. *J. Phys. Chem.* **1989**, *93*, 5188.

(47) Hunnicutt, S. S.; Waits, L. D.; Guest, J. A. *J. Phys. Chem.* **1991**, *95*, 562.

(48) Peterman, D. R.; Daniel, R. G.; Horwitz, R. J.; Guest, J. A. *Chem. Phys. Lett.* **1995**, *236*, 564.

(49) Feller, D.; Dixon, D. A.; Fransico, J. S. *J. Phys. Chem. A* **2003**, *107*, 1604. Domalski, E. S.; Hearing, E. D. *J. Phys. Chem. Ref. Data* **1993**, *22*, 805−1159. Baulch, D. L.; Cobos, C. J.; Cox, R. A.; Esser, C.; Frank, P.; Just, Th.; Kerr, J. A.; Pilling, M. J.; Troe, J.; Walker, R. W.; Warnatz, J. *J. Phys. Chem. Ref. Data* **1992**, *21*, 411. Rui, M. B. D. S.; Jose, A. M. S. *J. Phys. Chem. Ref. Data* **1998**, *27*, 707.

(50) Fang, W.-H.; Liu, R.-Z.; Zheng, X.; Phillips, D. L. *J. Org. Chem.* **2002**, *67*, 8407.

(51) Duncan, T. V.; Miller, C. E. *J. Chem. Phys.* **2000**, *113*, 5138.

(52) Li, Y.; Francisco, J. S. *J. Chem. Phys.* **2000**, *113*, 7963.